Hindawi
Advances in Civil Engineering
Volume 2022, Article ID 7761639, 13 pages
https://doi.org/10.1155/2022/7761639

Research Article

Investigating the Frequency Spectrum Characteristic of Stress Wave under Multistage Loading Stress

Yun Cheng,[1,2] **Zhanping Song**,[2,3] **Xiaoxu Chang**,[4] **and Tengtian Yang**[5]

[1]*School of Civil Engineering, Yancheng Institute of Technology, Yancheng 224051, China*
[2]*Shaanxi Key Laboratory of Geotechnical and Underground Space Engineering, Xi'an 710055, China*
[3]*School of Civil Engineering, Xi'an University of Architecture and Technology, Xi'an 710055, China*
[4]*Henan Land Rel Estate Group Co., Ltd., Zhumadian, Henan 463000, China*
[5]*China Railway Bridge Engineering Bureau Group Co., Ltd., Tianjin 300300, China*

Correspondence should be addressed to Yun Cheng; chengyun_ifu@163.com and Zhanping Song; songzhpyt@xauat.edu.cn

Received 13 October 2022; Revised 11 November 2022; Accepted 22 November 2022; Published 14 December 2022

Academic Editor: Jian Zhang

The stability of rock mass is destroyed by natural or human activities and leads to stress redistribution, causing the rock mass in a certain stressful environment. This study conducted a small disturbance impact tests on sandstone bar under loading stress by modified split Hopkinson pressure bar (SHPB). The results show that the reflection and transmission characteristics of stress wave are affected due to the loading stress changes in the sandstone porosity. The loading stress has a specific effect on the frequency spectrum distribution of the stress wave. The frequency spectrum curve has gone through the three stages, a gradual increase, then rapid attenuation, and finally a smooth development with the frequency increasing, and its dominant frequencies are mainly concentrated in 0~2 kHz. The loading stress has a significant influence on the variation tendency of the dominant frequency. The dominant frequency experiences a slow increase and then tends to be stable, and the total energy of the frequency band shows a fast attenuation and then a gentle development, and its stress boundary point is $\sigma/\sigma_c = 30\%$. The total energy attenuates as a first-order exponential function and its attenuation rate shows an exponential-linear function with the increasing loading stress, the farther away from the shock end, the faster the total energy attenuation is. The sandstone can filter the high-frequency wave and the low-frequency wave can penetrate rock media better. The closer the distance to the impact source, the greater the total energy of the frequency band. The frequency band energy is mainly concentrated in 0~36.62 kHz, the higher the frequency of the frequency band is, the smaller the energy ratio is. Therefore, those conclusions can provide a reference for the evolution analysis of the stress wave spectrum in an excavated rock mass.

1. Introduction

Rock mass activities and stress wave motions caused by rock blasting, mechanical drilling, and ore-body vibration are the fundamental physical phenomenon, such as tunnel excavation and mining engineering [1–6]. To achieve the purpose of reducing disaster prevention and efficient construction, studying on the propagation characteristics of stress wave in rock mass has never stopped and because the energy attenuation essentially causes the stress wave attenuation. Therefore, rock mass instability caused by natural or human activities is studied due to that behaviour not only destroys the stress balance of the original rock but also leads to the phenomenon of stress redistribution [7–12].

The blasting signal has the characteristic of short duration and which is a local nonstationary signal integrating the time-domain and frequency-domain [13], so it is difficult to observe the distribution characteristics of vibration frequency and spectrum energy in the time-domain due to the complexity of the frequency component of the stress wave signal. Studying the blasting and vibration signal is an essential part of the blasting vibration field [14]. The wavelet analysis provides a new method for the inversion of real waveform and analysis of frequency-domain characteristics [15]. The wavelet analysis has been

applied in engineering detection [16, 17] and rock mass blasting [18, 19]. However, the order of frequency band obtained by wavelet packet transformation is not consistent with the node order due to the limitation of a mathematical algorithm, and there will be the phenomenon of frequency hopping [20]. If this problem is ignored, the frequency band can not be accurately located and which will affect the correctness of the subsequent time-frequency analysis. Therefore, it is of considerable significance to clarify the corresponding relationship between the frequency band and node order in the wavelet packet tree for time-frequency analysis. Chen et al. [21] decomposed and reconstructed the measured wave signal of blasting vibration, and then obtained the time signal and spectrum of the reconstructed sub-band. Zhao et al. [22] found that the total energy and duration of the main frequency increase almost linearly [23]. Zhang et al. [20] put forward a method of predicting the dominant frequency and vibration spectrum curve according to particle displacement, vibration velocity, and acceleration spectrum. Triviño et al. [24] studied the influence of different blasting conditions on the signal frequency and energy variation and introduced the concept of average frequency. Song and Cao [25] put forward the safety criterion and damping measures of blasting vibration in surrounding rock.

The spectrum characteristics of the stress wave reflect the essential information of rock damage and the research has essential theory and application value. Jia et al. [26] analyzed the original waveform characteristics and two-dimensional spectrum characteristics and sought the intrinsic frequency spectrum of burst time. Jin et al. [16] analyzed the main frequencies and spectrum shapes of the reflected and transmitted wave under confining pressure. It can be seen that the distribution characteristics of the spectrum and spectrum energy of shock wave signal have been paid more attention from different angles, which is of great theoretical and practical significance for safe blasting excavation of rock mass. However, the distribution characteristics of the frequency spectrum and frequency band energy of rock stress wave under different loading stresses have not been reported. The split Hopkinson bar (SHPB) is the most commonly used technique for investigations of rock properties and its shock wave propagation problem under impact loading [17]. A typical SHPB consists of a striker bar, incident bar, and output bar. A rock sample is placed between the incident bar and output bar, and a striker bar shocks one end of the incident bar to generate a compression wave. The compression wave propagates through the incident bar toward the other end that interfaces the specimen. The strain gauges are usually pasted on the incident bar and transmission bar to capture the shock wave signal under the impact action. The above-given process is how an impact compression wave is applied to a rock sample. The attenuation characteristics of stress wave in whole deformed rock cannot obtain, and the rock with a more significant length: diameter ratio can achieve the expected effect by setting multiple testing points measuring several multidata of stress wave signals simultaneously [27].

In this study, experiments were conducted to design a sandstone bar with a length-diameter ratio of 65 and gradually load 13 different loading stresses by a modified SHPB, followed by an analysis concerning the wave shape characteristic from the viewpoint of temporal-spatial attenuation characteristic. Then, the distribution characteristics of frequency-domain, frequency spectrum, and frequency band energy of stress wave under loading stress condition were studied based on experimental data. It is hoped that these experimental conclusions can provide a practical reference for the evolution analysis of the frequency spectrum of stress wave in the excavated rock mass.

2. Experimental Schemes

2.1. Monitoring Apparatus. The SHPB system has the function of loading static stress and dynamic loading, which can provide the monitoring possibility of stress wave propagation in rock. The experimental system is mainly composed of axial loading device, velocimeter device, dynamic loading device, data acquisition, and display equipment, as shown in Figure 1. Because of the large length-diameter ratio of a rock sample, the traditional experimental principle of SHPB is no longer suitable for this test [18]. Therefore, multiple strain gauges are bonded directly to the sample surface to capture the stress wave signal under each loading stress. The diameters of the incident bar and transmission bar of the SHPB test system are 50 mm, and their lengths are 2000 mm and 500 mm, respectively.

The apparatus parameters are summarized as follows:

(i) The axial loading device is controlled by a hydraulic pump to realize the loading of static stress. The loading range of the hydraulic pump is 0~25 MPa, and its minimum scale is 0.50 MPa. The oil pressure is set to 0 MPa, 1, 2, 3, . . ., n MPa. The maximum oil pressure n is related to the maximum compressive strength (σ_m) of the sandstone bar.

(ii) The velocimeter device is composed of JXCS-02 chronograph, laser emission, and receiving device. The monitoring range and resolution ratio are 0.1~99999.9 μs and $\pm$0.1 μs, respectively. The velocimeter device can be used to measure the impact velocity of the striker bar.

(iii) The dynamic loading device includes impact bar, high pressure gas, and launching cavity. The high pressure air can provide impact kinetic energy for the striker bar in the launching cavity, and the stress wave generated is input into the sandstone bar. The striker bar can load a half-sine wave and eliminate Pochhammer–Chree oscillation [3, 16].

(iv) The data acquisition equipment is an SDY2017A dynamic strain meter with the strain coefficient and sensitivity of 2.00 k and 0.001 V/$\mu\varepsilon$. The stress wave signals in the sample can be collected by the connection of a dynamic strain meter and strain gauge, and its sampling time ranges from -100 μs to 900 μs. The data display equipment is a YokowagaDL850E

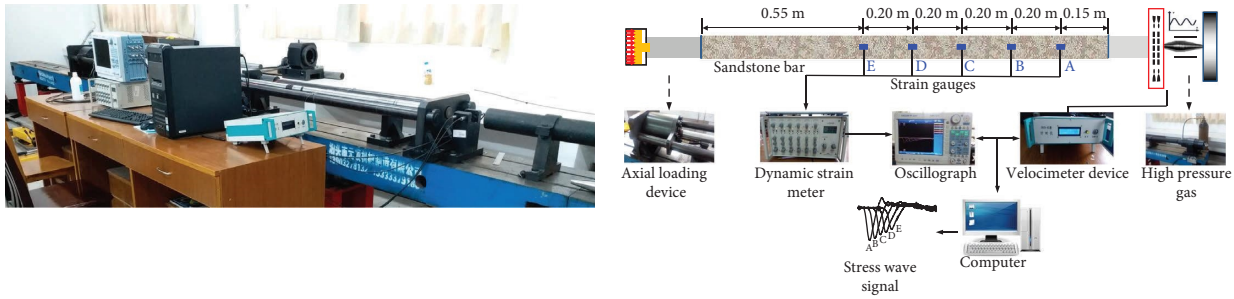

Figure 1: Diagram of experimental system.

oscilloscope with a signal amplification function, the testing accuracy, conversion resolution are 0.005%, 12 bit A/D, respectively.

2.2. Experimental Material. The sample was taken from the Huaping quarry in Ganzhou, China. The sandstone is red and has excellent integrity and homogeneity. The longitudinal wave velocity, density, particle size, and original porosity are 2390.00 m/s, 2.35 g/cm^3, 5.22%, and 0.05~2.00 mm, respectively. Fluorescence Spectrophotometry testing shows that the main mineral composition is quartz (SiO_2) with the composition content of 76.80%. Figure 2 shows the stress-strain curve of the standard sample (Φ50 mm × 100 mm) [3], indicating that the failure process experiences the compaction (OP), elastic deformation (PQ), cracks development, and expansion (QM) and failure stages (MN). The uniaxial compressive strength (σ_c) and elastic modulus (E) are 52.00 MPa, and 5.65 GPa, respectively.

To obtain the stress wave under different loading stresses and investigate the distribution characteristics of the frequency spectrum and frequency band energy, it is necessary to consider three factors including multipoint arrangement, sandstone brittleness, and loading stress range [17]. For the experimental purpose, the following measures are taken:

(i) Multiple groups of stress wave signals need to be tested under each loading stress, and the rock sample should be designed as a larger length-diameter ratio to stick to various strain gauges.

(ii) Considering the brittle failure characteristics and processing difficulty of sandstone material, the sample is processed into a sandstone bar with a section of 80 mm × 80 mm and a length of 1500 mm after exploration tests, its end smoothness less than 0.02 mm.

(iii) The critical instability stress of a larger length-diameter ratio is lower than that of the standard sample (Φ50 mm × 100 mm), so it is also necessary to test the maximum loading stress (critical instability stress) of the sandstone bar. The sandstone bar is fixed between incident bar and transmission bar, and the axial loading device loads the loading stress according to the test scheme. Three small disturbance impact tests are carried out under each axial loading stress. The sandstone bar is destroyed (as shown in Figure 3) when the axial loading stress is 39.00 MPa. The critical instability stress is 39 MPa.

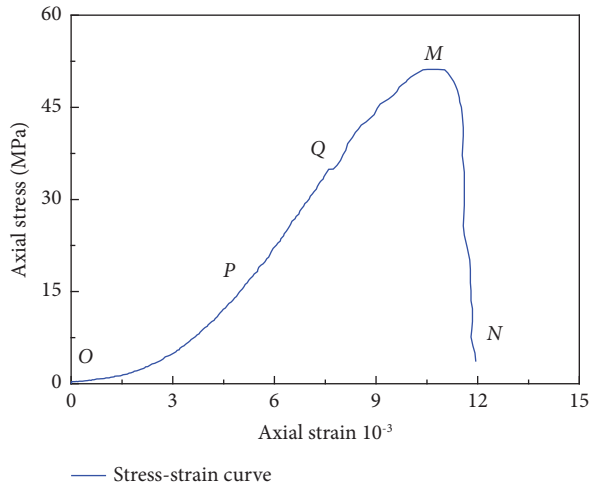

Figure 2: Stress-strain curve of standard sandstone.

It should point out that the proportional coefficient between the cross-sectional area of the oil inlet pipe in the hydraulic pump and effective cross-sectional area of the sandstone bar is 1 : 2.76. The maximum oil pressure n is set to 12 MPa, that is, the maximum loading stress can be determined as 2.76 × 12 MPa = 33.12 MPa < 39.00 MPa. Therefore, the loading stresses (σ) of the sandstone bar are 0, 2.76, 5.52, 8.28, ..., 24.84, 27.60, 30.36, 33.12 MPa. The relationship between loading stress and oil pressure satisfies $\sigma = 2.76n$.

2.3. Experimental Procedure. To obtain the stress wave signals under different loading stresses, the experimental procedure and principle are as follows:

(i) Strain gauges are arranged equally spaced on the rock surface. Arrange five strain gauges (A, B, C, D, and E) on the sample surface. Two longitudinally symmetric strain gauges are attached to each testing point to lower the error, its resistance value, size, supply voltage, sensitivity coefficient, and strain limit are 120 ± 1 Ω, 8 mm × 5 mm, 3~10 V, ±2.0% and strain limit are 20000 μm/m, respectively.

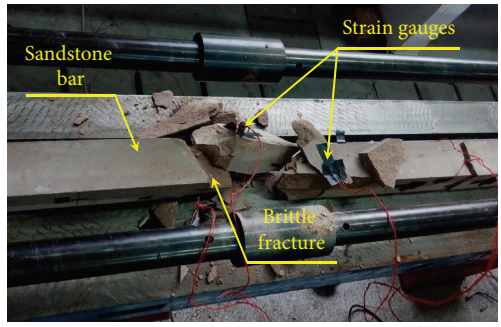

Figure 3: Critical instability of sandstone bar.

(ii) The sandstone bar is assembled onto the SHPB system. Two steel pads with coupling agents are added to the interfaces between the sandstone bar and incident bar (transmission bar) to prevent the occurrence of stress concentration phenomenon and reduce inter-facial friction, ensuring the excellent transmission of stress waves.

(iii) Connect the strain gauge and stress load. The sandstone bar is loaded to a certain value by the axial loading device. Three impact tests of the same strike strength under each loading stress are carried out and save the stress waves. The previous study has shown that when stress wave amplitude is less than 60% of uniaxial compressive strength, the damage caused by the cyclic stress wave could be ignored [28]. The strength of high pressure gas is set to 0.25 MPa to achieve an impact velocity of 4.38 m/s. The impact velocity is measured by a velocimeter device.

3. Results and Discussions

3.1. Wave Shape Characteristic and Band Selection of Stress Wave. It is a feasible and effective method to study the propagation characteristics of stress wave or shock wave by measuring the voltage signal when the parameters such as stress and strain in rock can not be measured [28]. Figure 4 shows the typical stress wave with a loading stress of 0, 2.76, 11.04, 19.32, 27.60, and 33.13 MPa. The stress wave amplitudes are characterized by the voltage values, and the positive and negative ordinate indicate the tensile wave and compression wave.

Figure 4 shows that the presence or absence of loading stress has a significant effect on the wave propagation of stress wave. When there is no loading stress, only a compression wave exists and almost no tensile wave, this is due to the primary pores are present in the sample and without secondary pores, and the reflection phenomenon of stress wave in the pore interface is not apparent. When the loading stress is more than 0 MPa, the tensile wave appears in the tail of the stress wave at each test point, and the larger the loading stress, the more obvious the tensile amplitude occurs. Besides, with increasing time, the stress wave first jump along the negative direction to reach the compression wave, then the stress wave continues to climb to form a tensile wave, and then tends to be stable gradually, showing the coexistence of compression wave and tensile wave. Moreover, under the same loading stress, with increasing propagation distance, the compression wave peak decreases gradually, and the waveform is similar.

The compression wave caused by explosion or impact actions will occur the transmission and reflection phenomenon at the rock pore or fracture interface [29], its transmission coefficient and reflection coefficient are related to the wave impedance and rock porosity. During the stress wave propagation, the compression wave and tensile wave will produce compression stress and tensile stress, thus leading to the rock being subject to the repeated compression-tension effect and the rock will cause failure when this compression-tension action reaches a critical failure extent. Figure 4 indicates that with increasing propagation time, the compression wave input by the impact bar is gradually transformed into a tensile wave and there is an obvious delay phenomenon between the compression wave peak and tensile wave peak, and the delay characteristics are significantly affected by the loading stress. The temporal-spatial attenuation law, the waveform characteristics, and the energy dissipation of stress wave have been presented in other papers. It is necessary to analyse the frequency spectrum distribution and variation law of frequency band energy in the process of converting a compressed wave into a tensile wave. Because the experimental acquisition time is much longer than the stress wave delay and meanwhile to refine the stress wave data, so we select the appropriate waveband data to conduct the wavelet decomposition. The waveband data of wavelet decomposition are shown in Table 1, the starting point and ending point of the waveband are the compression wave peak and tensile wave peak, respectively. The working condition 63~522 μs is a good example when the loading stress is 0 MPa at strain gauge A, indicating that the starting point and ending point are 63 μs and 522 μs, respectively.

3.2. Frequency Spectrum Distribution Characteristics. The loading stress has a significant effect on the stress waveform, and the waveform change in time-domain is closely related to the distribution characteristics of the frequency spectrum in frequency-domain. The stress wave is composed of high-frequency wave and low-frequency wave, and the stress waves in different frequency bands correspond to different attenuation characteristics [30]. The corresponding frequency spectrum curves are obtained by the fast Fourier transform to reveal the frequency spectrum characteristics, as shown in Figure 5. The maximum amplitude of the frequency spectrum is called the dominant frequency peak, and the frequency corresponding to the maximum amplitude is called the dominant frequency.

It is can be seen from Figure 5 that the loading stress has a certain influence on the frequency spectrum distribution of the stress wave. The following conclusions can be summarized: (1) the frequency spectrum shape and its development trend are similar under arbitrary loading stress. The frequency spectrum curve has gone through the three stages, a

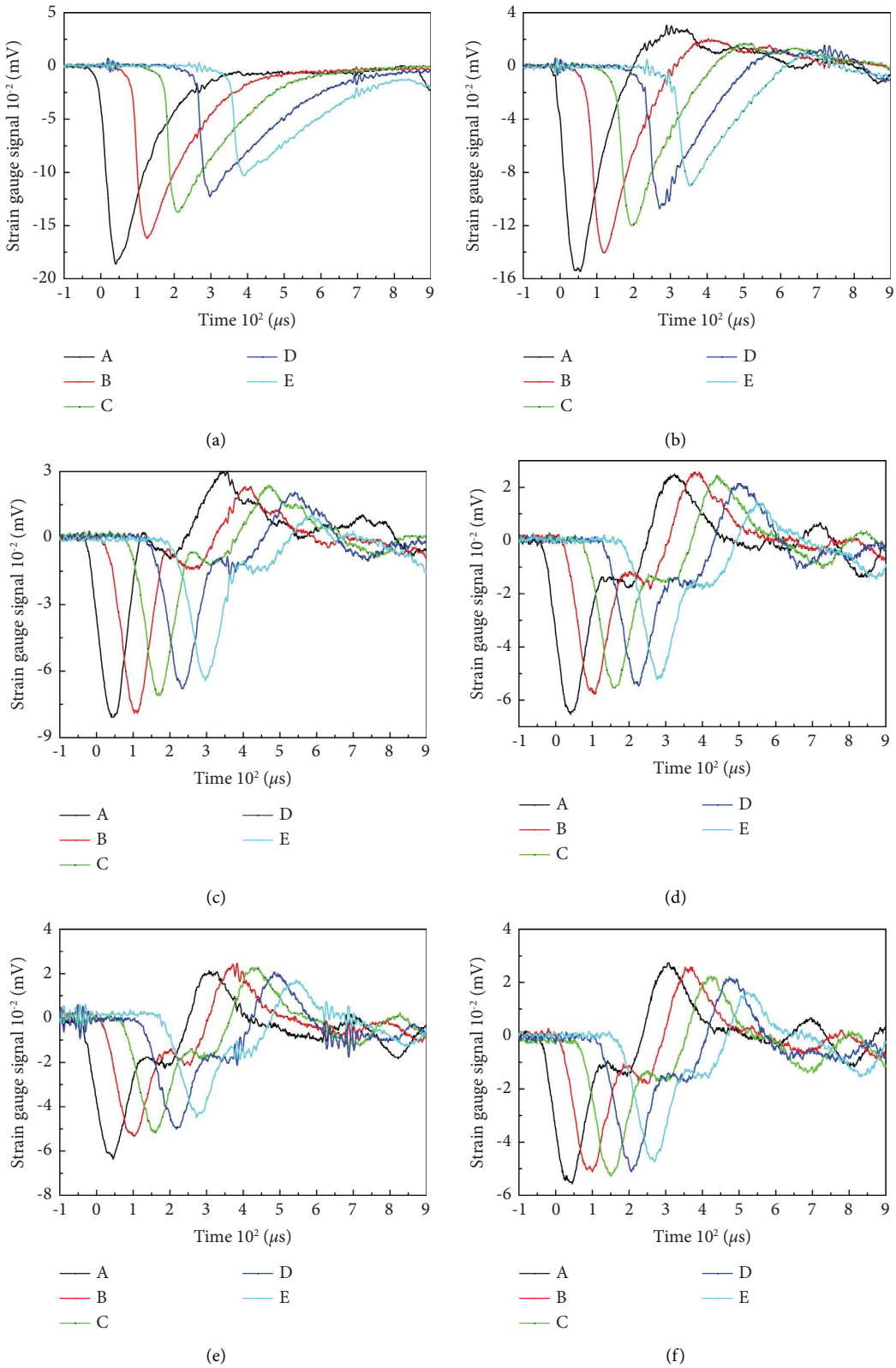

Figure 4: Stress waves under different loading stresses [14]. (a) 0 MPa. (b) 2.76 MPa. (c) 11.04 MPa. (d) 19.32 MPa. (e) 27.60 MPa. (f) 33.12 MPa.

Table 1: Waveband data of wavelet decomposition.

Loading stress (MPa)	Waveband data (μs)				
	A	*B*	*C*	*D*	*E*
0	63~522	143~584	209~751	301~843	364~906
2.76	82~405	133~499	196~581	260~684	308~765
5.52	76~311	118~386	187~470	269~533	298~619
8.28	63~260	122~327	178~400	249~470	298~532
11.04	70~457	123~504	181~569	237~642	293~685
13.80	66~422	118~489	172~554	222~613	268~678
16.56	61~415	120~484	175~541	227~602	290~667
19.32	61~425	119~478	176~541	230~597	281~649
22.08	61~417	116~479	166~534	230~592	282~652
24.84	56~407	118~474	165~523	218~590	280~639
27.60	50~408	110~484	161~524	214~585	275~645
30.36	57~400	113~477	165~514	217~589	290~633
33.12	57~400	113~477	165~514	217~589	290~627

gradual increase, then rapid attenuation, and finally a smooth development with increasing of frequency, this phenomenon can be explained through one-dimensional stress wave theory [31]. Since the stress waves under the different loading stresses have the same shock strength, the stress waves in the same time-domain also have the similar characteristics in frequency-domain, which is consistent with results obtained by Jin et al. [16]. (2) The dominant frequency peak of the frequency spectrum curve is more prominent under the same loading stress, and there is almost no secondary dominant frequency, and the dominate frequency of the stress wave is concentrated in 0~2 kHz segment of relatively low frequency. The frequency spectrum curve gradually approaches to 0 mV when the frequency in the 4~10 kHz stage. (3) The peak value of the main frequency of stress wave decreases gradually with the increasing propagation distance and loading stress, and the attenuation degree is related to the evolution of sandstone porosity.

3.3. Effect of Loading Stress on Dominate Frequency. Figure 6 shows the variation tendencies of the dominant frequency with the increasing loading stress at different strain gauges, indicating that the loading stress has a significant influence on the dominant frequency of the stress wave. The development trend of the dominant frequency variation curve at different points is similar, and all experience a slow increase first then tends to be stable. If the ratio of loading stress (σ) to uniaxial compressive strength (σ_c) is selected as the judging basis, the stress boundary point of the above-given two stages of dominant frequency variation curve is $\sigma/\sigma_c = 30\%$, which is consistent with the demarcation points of the stress wave peak [3].

The dominant frequency variation characteristics of the nonlinear stage and linear stage are analyzed as follows: when σ/σ_c is less than 30%, although the dominant frequency has a certain degree of discrete characteristics, it tends to nonlinearity increases slowly with different intensities with the growth of loading stress. This is because the sandstone interior appears to the compression of primary pores and the readjusting of local fracture structure during the stress strengthening stage with increasing loading stress, causing the transmission and reflection ability of stress wave. The decreased porosity leads to the slowing down of the pore absorption ability of stress wave energy, then causes the dominant frequency to increase slowly. As the loading stress continues to increase, the dominant frequency gradually tends to stable development when the stress ratio is more than 30%, and its variation range is 0.60~1.20 kHz. This is because with increasing loading stress, the number of closed pores and new pores in sandstone is approximately equal, the number of the total pores is in a relatively stable state, and the absorption degree of stress wave energy is gradually steady, which leads to a smaller range fluctuation of the dominant frequency.

Besides, it is found that the closer the measuring point is to the incident end of sandstone compared with the dominant frequencies under the same loading stress, the larger the dominant frequency value is. The reasons for this are that the collected stress wave signals are mainly broadband waves consisting of different frequencies and at different attenuation levels. It is generally believed that the attenuation intensities of high-frequency stress waves are higher than those of low-frequency stress waves [32]. High-frequency waves are absorbed through pores or damage in sandstone, and relatively fewer high-frequency stress waves are intercepted at later test points. This also suggests that the sandstone under different loading stresses has a filtering action on high-frequency stress wave with a varying degree. The above analysis has shown that the increased loading stress leads to the change of porosity and which causes to the nonlinear and linear stages of the dominant frequency. The variation tendencies of dominant frequency also signify that the frequency spectrum of stress wave has a different sensitivity to different loading stress range. The regression analysis shows the exponential function can well describe the relationship between dominant frequency and loading stress.

Figure 7 exhibits the variation tendency of decay rate (V_{fd}) of dominant frequency calculated by $(f_{dA} - f_{dE})/0.80$, f_{dA} and f_{dE} are the dominant frequencies of strain gauges *A* and *E*, 0.80 (m) is the distance from strain gauges *A* and *E*. It can be concluded that the decay rate of the dominant frequency decreases gradually with the increasing loading stress, the decay rate of the dominant frequency has a higher dispersion degree but decreases nonlinearly as a whole in the low-stress region. In the high-stress region, the dispersion degree of decay rate with the increasing loading stress is gradually reduced, showing a typical linear attenuation. The demarcation point of high-stress region and low-stress region is roughly $\sigma/\sigma_c = 30\%$, which is consistent with the previous analysis. Furthermore, a linear-exponential function is given to describe the relationship between the decay rate of dominant frequency and loading stress.

3.4. Frequency Band Energy Characteristics

3.4.1. Band Decomposition and Reorder of Frequency Band. The number of decomposition layers should be determined according to the measured stress wave signal and sampling

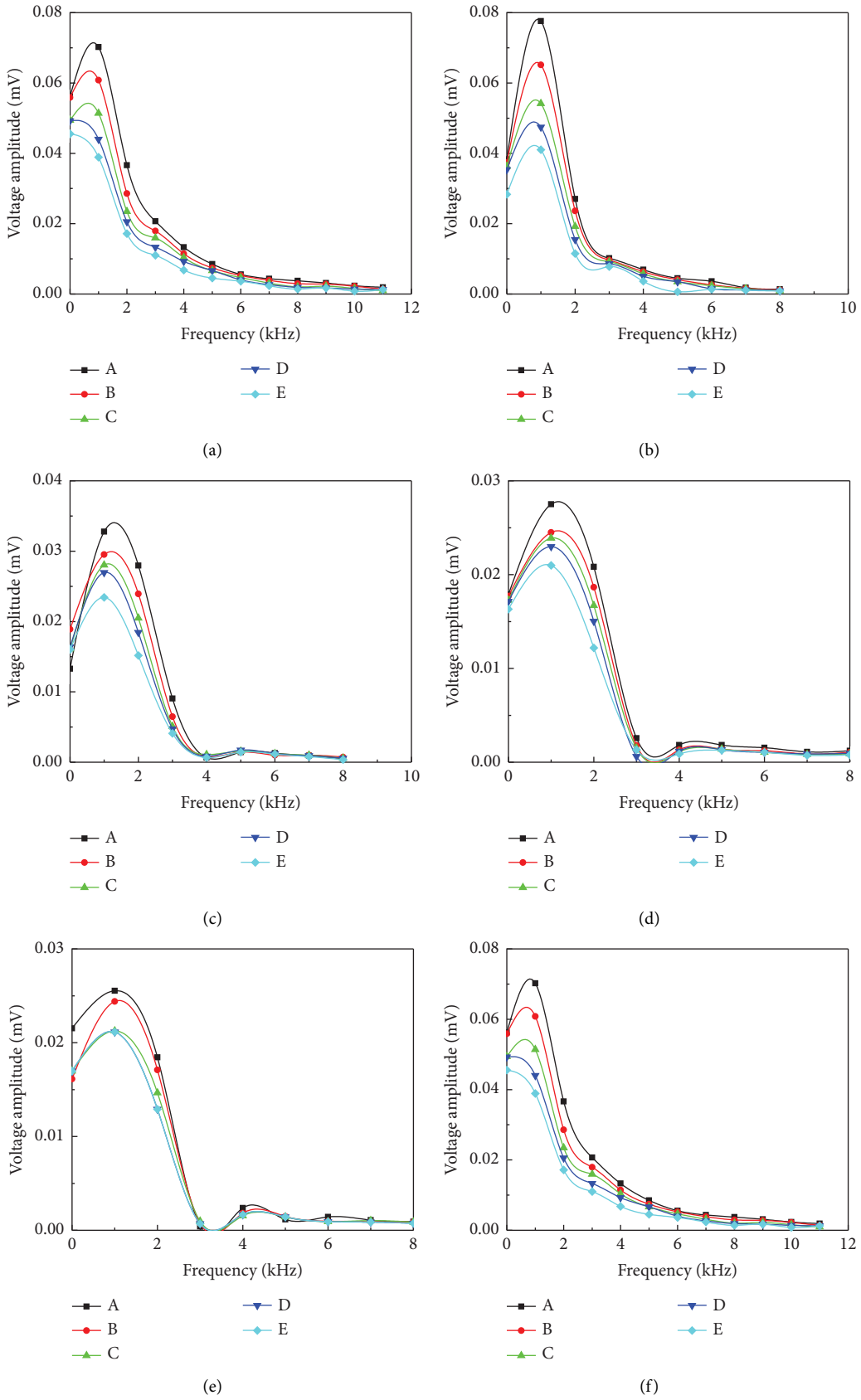

Figure 5: Frequency spectrum curves of stress wave. (a) 0 MPa. (b) 2.76 MPa. (c) 11.04 MPa. (d) 19.32 MPa. (e) 27.60 MPa. (f) 33.12 MPa.

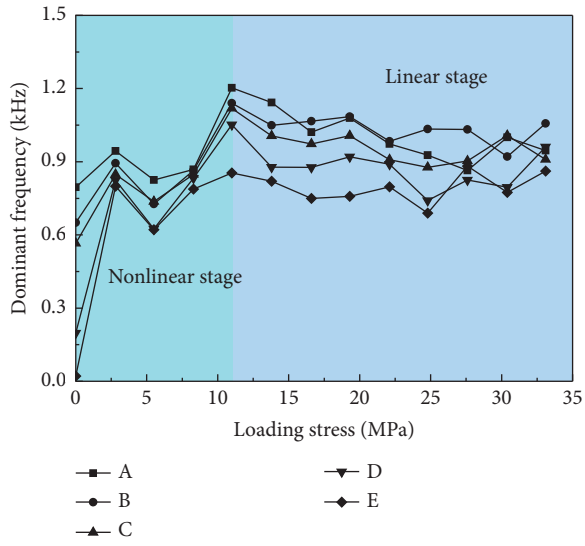

Figure 6: Variation tendencies of dominant frequency.

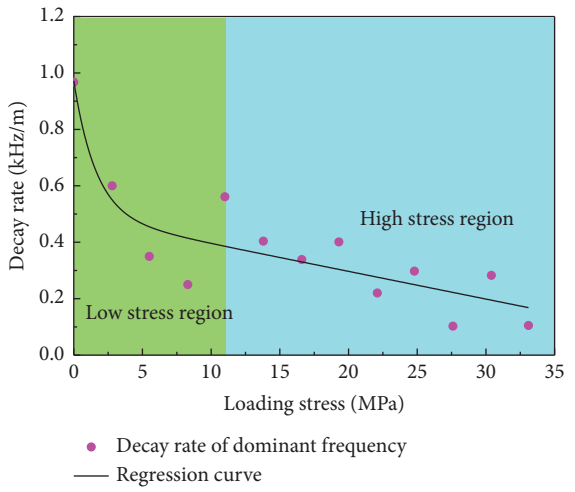

Figure 7: Variation tendency of decay rate of dominant frequency.

frequency when the stress wave signal is decomposed by a wavelet packet. Considering the half-sine wave of the same impact strength and the sampling frequency is 1 MHz, the Nyquist frequency is 500 kHz based on sampling theory [33]. Therefore, the collected stress wave signal is decomposed in 12 layers, including 4096 wavelet packets, each wavelet packet coefficient corresponds to one frequency band, and the bandwidth corresponding to each node in layer 12 is 122.07 Hz. The wavelet packet coefficients are ordered according to the Parlay order [23], causing the frequency band of layer 12 sorting for x (12, i) (i = 1~4095) after wavelet packet decomposition is not a strict sequence of natural number increments. The nonincremental coefficients need to be rearranged, which is indicated as N (i) (i = 1~4095). The reordering coefficients after wavelet packet decomposition are obtained according to the decomposition algorithm of wavelet packet based on MATLAB programming, and simultaneously the reorder of the frequency band range from low to high are shown in Table 2.

Table 2: Reorder of frequency band range.

Node order	Frequency order	Frequency band range (Hz)
N (0)	x (12, 0)	0~122.07
N (1)	x (12, 1)	122.07~244.14
N (2)	x (12, 3)	244.14~366.21
N (3)	x (12, 2)	366.21~488.28
N (4)	x (12, 6)	488.28~610.35
N (5)	x (12, 7)	610.35~732.42
N (6)	x (12, 5)	732.42~854.49
N (7)	x (12, 4)	854.49~976.56
N (8)	x (12, 12)	976.56~1098.63
N (9)	x (12, 13)	1098.63~1220.70
...	...	...
N (4090)	x (12, 2055)	499266.30~499388.37
N (4091)	x (12, 2054)	499388.37~499510.44
N (4092)	x (12, 2050)	499510.44~499632.51
N (4093)	x (12, 2051)	499632.51~499754.58
N (4094)	x (12, 2049)	499754.58~499876.65
N (4095)	x (12, 2048)	499876.65~500000.00

3.4.2. Effect of Loading Stress on Frequency Band Energy. The decomposition coefficients of the frequency band can be reconstructed after wavelet packet decomposition, and then the stress waves of different frequency bands can be extracted to realize the analysis of frequency band energy. The frequency band energy of the stress wave is defined as the square of the amplitude, and the frequency band j of layer 12 is represented as $S_{12,j}$. The frequency band energy can be expressed as follows:

$$E_{12,j} = \int \left|S_{12,j}(t)\right|^2 \mathrm{d}t = \sum_{k=1}^{m} \left|x_{j,k}\right|^2, \quad (1)$$

where $x_{j,k}$ represents the discrete amplitude of the reconstructed signal $S_{12,j}$, j = 0, 1, 2, ..., 2^{12-1}; k = 1, 2, ..., m; m represents the sampling number.

The total energy (E_f) of the frequency band can be expressed as follows:

$$E_f = \sum_{j=0}^{2^{12-1}} E_{12,j}. \quad (2)$$

The energy ration of the frequency band can be written as follows:

$$E_j = \frac{E_{12,j}}{E_f} \times 100\%. \quad (3)$$

Figure 8 shows the variation tendency of total energy with the increase of loading stress, indicating that the total energy of the frequency band has a similar development trend, and all experience a first rapid attenuation and then a smooth development. The stress boundary point of the two stages is σ/σ_c = 30%, which is the same as the stress boundary point of the variation tendency of the dominant frequency. The relative variation of the total energy of the frequency band is 41.69~49.98% when the stress ratio σ/σ_c is increased from 0 to 30%, showing a significant nonlinear attenuation. There are only 0.56~12.26% relative variation of total energy

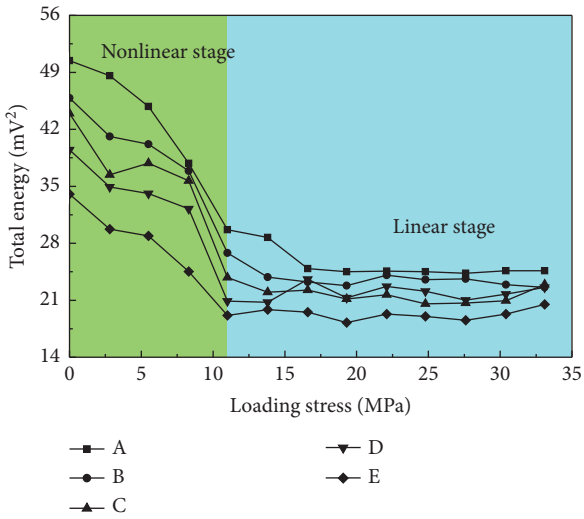

Figure 8: Variation tendency of total energy with the increase of loading stress.

when the stress ratio σ/σ_c is more than 30% and which has a stable linear development.

In addition, Figure 8 manifests that the total energy of the frequency band under the same loading stress satisfies $E_{fA} > E_{fB} > E_{fC} > E_{fD} > E_{fE}$ with the increase of propagation distance. To characterize the attenuation degree of total energy with the increase of loading stress, the regression analysis shows that the relationship between total energy and loading stress is an exponential function. Regression parameters are shown in Table 3. E_{f0}, E_{f1} are the regression parameter related to loading stress. R_0 is the attenuation coefficient, representing the decay degree of the total energy of the frequency band. It is can be seen that the attenuation coefficient increases with the increase of propagation distance, indicating that the farther away from the shock end, the faster the total energy attenuation of the frequency band is.

$$E_f = E_{f0}e^{-R_0\sigma} + E_{f1}. \quad (4)$$

To study the decay rate of the total energy of the frequency band with the increasing loading stress, the decay rate is defined as $\eta_0 = (E_{OA} - E_{OE})/E_{OA}$, E_{0A}, and E_{0E} are the total energy of the strain gauges A and E. Figure 9 shows the relation between the decay rate of total energy and loading stress, revealing that the decay rate is slowly attenuated by oscillating as a whole with the increasing loading stress, and gradually tends to be stable when the stress ratio is $\sigma/\sigma_c = 30\%$. The regression equation shows that the relation between the decay rate of total energy and loading stress is an exponential-linear function, the attenuation coefficient, and correlation coefficient are 0.0040 and 0.7366, respectively.

3.4.3. Effect of Propagation Distance on Frequency Band Energy. Figure 10 shows the total energy under different loading stresses. The regression analysis shows that the total energy of the frequency band decreases linearly of different intensities with the increase of propagation distance, the

Table 3: Relevant parameters of regression equation.

Strain gauges	$E_{f0} \times 10^2$	R_0	$E_{f1} \times 10^2$
A	0.3332	0.0823	0.2006
B	0.2642	0.0967	0.2056
C	0.2569	0.1049	0.1923
D	0.2015	0.1227	0.2064
E	0.1601	0.1293	0.1821

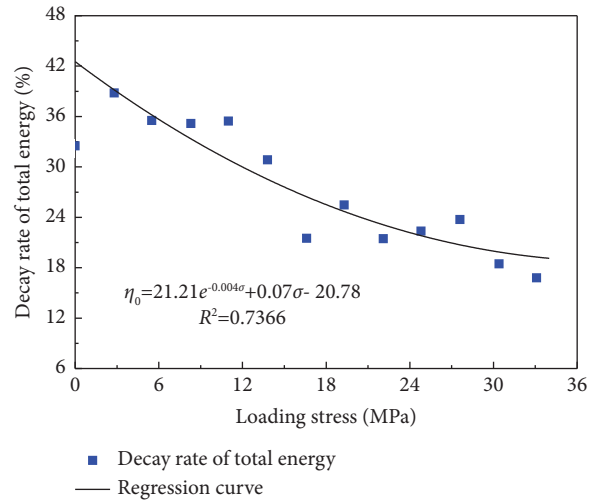

Figure 9: Relation between decay rate of total energy and loading stress.

linear slope is between 4.14 and 21.94. The linear slope can characterize the attenuation intensity of total energy, it is found that the attenuation intensity decreases gradually with the increasing loading stress, as shown in Figure 11.

It is can be seen that the evolution trend of attenuation intensity of total energy indicates that the attenuation intensity obviously experiences a fast attenuation first, and then gradually tends to be stable, having a similar development trend of the decay rate of total energy in Figure 9. The attenuation intensity decreases from 19.57 to 10.42 m^{-1} with an average attenuation rate is 17.80% when the stress ratio σ/σ_c is increased to 30%. The attenuation intensity decreases from 6.19 to 4.14 m^{-1} with an average attenuation rate is 6.76% when the stress ratio σ/σ_c is more than 30%. Therefore, whether the attenuation intensity or average attenuation rate, their values of the low-stress region is significantly greater than that of the high-stress region, which is related to the stress enhancement degree of sandstone [27, 28]. Besides, the stress boundary point of the variation trend of attenuation intensity is $\sigma/\sigma_c = 30\%$ and which is the same as Figure 7. The logarithmic function can reveal the statistical relationship between attenuation intensity and loading stress.

3.4.4. Effect of Loading Stress on Energy Ration of Frequency Band. The wavelet packet decomposition of the selected waveband data under different loading stresses is carried out by the Matlab program, which is decomposed into 12 layers including 4096 frequency bands with a bandwidth of

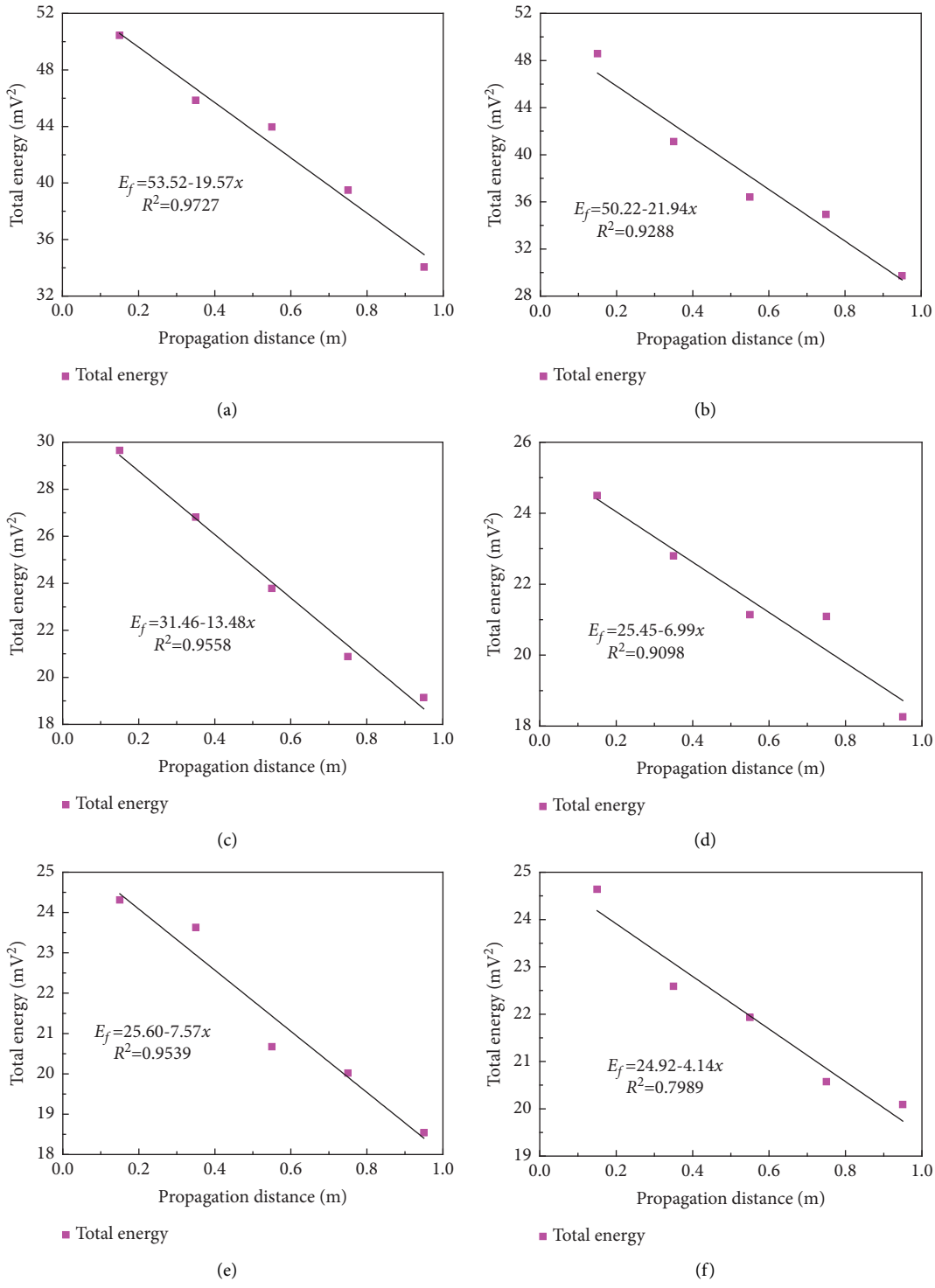

Figure 10: Total energy of frequency band. (a) 0 MPa. (b) 2.76 MPa. (c) 11.04 MPa. (d) 19.32 MPa. (e) 27.60 MPa. (f) 33.12 MPa.

122.07 Hz. However, it is found that the signal frequency of stress wave is mainly concentrated in the relatively lower-frequency region. So now with 300 frequency bands as a whole, the 4096 frequency bands are redivided into 14 frequency bands, 0~36.62, 36.62~73.24, 73.24~109.86, ..., 439.45~476.07, and 476.07~500 kHz, respectively. It should point out that the last frequency band only includes 196 bands, and its bandwidth is different from the first 13 bandwidths.

Table 4 shows the energy ratio of the frequency band at different strain gauges. It is can be seen that the energy ratios of the frequency band under any loading stress are mainly concentrated in the first frequency band 0~36.62 kHz, its energy ratios of corresponding loading stress from strain

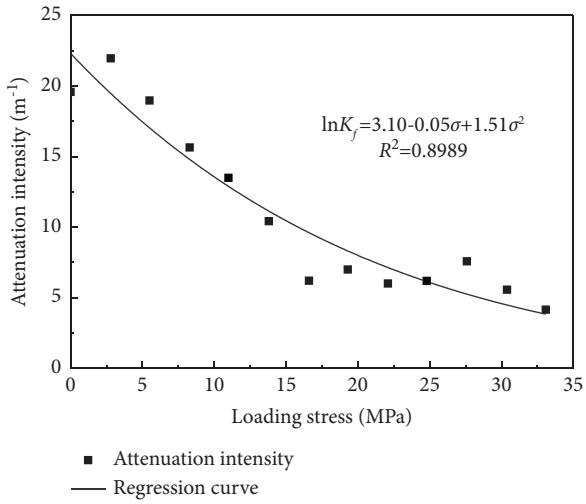

Figure 11: Relation between attenuation intensity and loading stress.

Table 4: Energy ration of frequency band.

Loading stress (MPa)	Frequency band (kHz)	Energy ratio (%)				
		A	*B*	*C*	*D*	*E*
0	0~36.62	91.05	89.7	87.91	86.41	86.71
	36.62~73.24	2.29	4.18	4.5	4.96	3.47
	73.24~109.86	1.31	1.58	1.81	2.16	1.99
	109.86~183.48	1.34	0.80	0.76	1.22	1.29
	...	...	...	...	...	...
	439.45~476.07	0.23	0.27	0.29	0.36	0.49
	476.07~500.00	0.25	0.23	0.36	0.26	0.71
5.52	0~36.62	92.94	92.89	87.88	81.1	80.77
	36.62~73.24	1.50	1.91	3.52	7.09	5.96
	73.24~109.86	1.05	0.71	2.15	4.18	3.04
	109.86~146.48	1.14	0.54	1.28	1.47	1.93
	...	...	...	...	...	...
	439.45~476.07	0.29	0.39	0.37	0.33	0.85
	476.07~500.00	0.19	0.18	0.18	0.24	0.92
11.04	0~36.62	86.15	83.79	84.53	80.88	80.21
	36.62~73.24	3.03	5.41	3.69	6.06	5.42
	73.24~109.86	1.91	2.30	1.44	2.63	2.70
	...	...	...	...	...	...
	439.45~476.07	0.54	0.73	0.89	0.74	0.60
	476.07~500.00	0.26	0.49	0.60	0.83	0.41
...	...	...	...	...	...	...
27.60	0~36.62	81.15	79.09	84.25	78.32	75.74
	36.62~73.24	4.46	5.08	3.29	7.23	6.15
	73.24~109.86	3.34	3.56	2.24	3.58	4.51
	...	...	...	...	...	...
	439.45~476.07	0.49	0.86	0.69	0.62	0.76
	476.07~500.00	0.43	0.57	0.47	0.42	0.49
33.12	0~36.62	85.23	84.25	79.09	73.65	73.99
	36.62~73.24	3.21	3.45	6.26	9.84	9.63
	73.24~109.86	2.14	2.86	3.37	5.23	4.29
	...	...	...	...	...	...
	439.45~476.07	0.55	0.68	0.89	0.65	0.53
	476.07~500.00	0.34	0.52	0.56	0.40	0.67

gauges A to E are 86.71~91.05%, 80.77~92.94%, 80.21~86.15%, 75.74~81.15%, and 73.65~85.23%, respectively. However, the energy ratios of the other frequency band are less than 5%. For the same strain gauge, the energy ratio decreases with the increase of frequency, the higher the frequency is, the smaller the energy ratio is; or else, the larger the energy ratio is. It can thus be concluded that the sandstone has a high-frequency filtering effect on stress wave, the higher-frequency stress wave will be filtered when it passes through sandstone fracture, and the lower-frequency stress wave has the strong penetration ability, which is consistent with the existing conclusion [32, 33].

4. Conclusions

Using Ganzhou sandstone in Jiangxi Province, China, as the test material, the wave shape characteristic, distribution characteristics of frequency-domain, frequency spectrum, and frequency band energy of stress wave under loading stress condition were studied based on the small disturbance impact tests with the same impact strength under different loading stresses. The conclusions can be drawn as follows:

(1) The reflection and transmission characteristics of stress wave are affected due to the loading stress changes in the sandstone porosity. The loading stress has a specific effect on the frequency spectrum distribution of the stress wave. The frequency spectrum curve has gone through the three stages, a gradual increase, then rapid attenuation, and finally a smooth development with the frequency increasing. The dominant frequency peak is more prominent, and there is almost no secondary dominant frequency, and the dominate frequency of stress wave is concentrated in 0~2 kHz segment of relatively lower frequency.

(2) The loading stress has a significant influence on the variation tendency of the dominant frequency. The dominant frequency all experiences a slow increase first then tends to be stable with increasing loading stress, and its stress boundary point is $\sigma/\sigma_c = 30\%$. The dominant frequency increases exponentially and its decay rate attenuates as a linear-exponential function as the loading stress increases, which signifies that the frequency spectrum of the stress wave has a different sensitivity to different loading stress range. The farther away from the shock end, the faster the total energy attenuation is. The attenuation rate of total energy attenuates shows an exponential-linear function revealing the relationship between attenuation intensity and loading stress.

(3) Sandstone has a high-frequency filtering effect on stress wave, the higher-frequency stress wave will be filtered when it passes through sandstone fracture, and the lower-frequency stress wave has a strong penetration ability. The stress wave energy under any loading stress is mainly concentrated in the first frequency band 0~36.62 kHz. The energy ratio decreases with increasing frequency. The higher the frequency is, the smaller the energy ratio is.

Data Availability

The data used to support the findings of this study are available from the corresponding author upon request.

Conflicts of Interest

The authors declare that they have no conflicts of interest.

Acknowledgments

The National Natural Science Foundation of China (Grant no. 52178393), the Science and Technology Innovation Team of Shaanxi Innovation Capability Support Plan (Grant no. 2020TD005), and Science and Technology Innovation Project of China Railway Construction Bridge Engineering Bureau Group Co., Ltd. (Grant No. DQJ-2020-B07).

References

[1] S. Y. Fan, Z. P. Song, T. Xu, K. Wang, and Y. Zhang, "Tunnel deformation and stress response under the bilateral foundation pit construction-a case study," *Archives of Civil and Mechanical Engineering*, vol. 21, no. 3, pp. 109–119, 2021.

[2] Z. P. Song, W. X. Song, Y. Cheng, T. Yang, T. Wang, and K. Wang, "Investigation on strain characteristics and fatigue constitutive model of limestone under osmotic pressure and cyclic disturbance coupling," *KSCE Journal of Civil Engineering*, vol. 26, no. 4, pp. 1740–1753, 2022.

[3] Y. Cheng, Z. P. Song, J. F. Jin, and T. Yang, "Attenuation characteristics of stress wave peak in sandstone subjected to different axial stresses," *Advances in Materials Science and Engineering*, vol. 2019, pp. 1–11, Article ID 6320601, 2019.

[4] Y. Cheng, Z. P. Song, T. T. Yang, J. Han, B. Wang, and Z. Zhang, "Investigating the aging damage evolution characteristics of layered hard sandstone using digital image correlation," *Construction and Building Materials*, vol. 353, pp. 128838–128919, Article ID 128838, 2022.

[5] K. Wu, Z. S. Shao, M. Sharifzadeh, Z. Chu, and S. Qin, "Analytical approach to estimating the influence of shotcrete hardening property on tunnel response," *Journal of Engineering Mechanics*, vol. 148, no. 1, Article ID 4021127, 2022.

[6] S. Y. Fan, Z. P. Song, T. Xu, and Y. Zhang, "Investigation of the microstructure damage and mechanical properties evolution of limestone subjected to high-pressure water," *Construction and Building Materials*, vol. 316, Article ID 125871, 2022.

[7] K. Wu, Z. S. Shao, M. Sharifzadeh, S. Hong, and S. Qin, "Analytical computation of support characteristic curve for circumferential yielding lining in tunnel design," *Journal of Rock Mechanics and Geotechnical Engineering*, vol. 14, no. 1, pp. 144–152, 2022.

[8] Z. P. Song, T. Wang, J. B. Wang, K. Xiao, and T. Yang, "Uniaxial compression mechanical properties and damage constitutive model of limestone under osmotic pressure," *International Journal of Damage Mechanics*, vol. 31, no. 4, pp. 557–581, 2021.

[9] C. Zhu, M. C. He, B. Jiang, X. Z. Qin, Q. Yin, and Y. Zhou, "Numerical investigation on the fatigue failure characteristics of water-bearing sandstone under cyclic loading," *Journal of Mountain Science*, vol. 18, no. 12, pp. 3348–3365, 2021.

[10] X. X. Tian, Z. P. Song, H. Z. Wang, Y. Zhang, and J. Wang, "Evolution characteristics of the surrounding rock pressure

and construction techniques: a case study from Taoshuping tunnel," *Tunnelling and Underground Space Technology*, vol. 125, Article ID 104522, 2022.

[11] N. F. Liu, N. Li, C. B. Xu, G. Li, Z. Song, and M. Yang, "Mechanism of secondary lining cracking and its simulation for the dugongling tunnel," *Rock Mechanics and Rock Engineering*, vol. 53, no. 10, pp. 4539–4558, 2020.

[12] N. F. Liu, N. Li, G. F. Li, Z. Song, and S. Wang, "Method for evaluating the equivalent thermal conductivity of a freezing rock mass containing systematic fractures," *Rock Mechanics and Rock Engineering*, vol. 55, no. 12, pp. 7333–7355, 2022.

[13] W. B. Lu, J. H. Yang, P. Yan et al., "Dynamic response of rock mass induced by the transient release of in-situ stress," *International Journal of Rock Mechanics and Mining Sciences*, vol. 53, no. 7, pp. 129–141, 2012.

[14] Y. Cheng, Z. P. Song, J. F. Jin, J. Wang, and T. Wang, "Experimental study on stress wave attenuation and energy dissipation of sandstone under full deformation condition," *Arabian Journal of Geosciences*, vol. 12, no. 23, pp. 736–750, 2019.

[15] M. Frisch and H. Messer, "The use of the wavelet transform in the detection of an unknown transient signal," *IEEE Transactions on Information Theory*, vol. 38, no. 2, pp. 892–897, 1992.

[16] J. F. Jin, C. Liang, J. Wang et al., "Effect of confining pressure on spectrum and frequency band energy of stress wave in red sandstone," *Nonferrous Metals Science and Engineering*, vol. 9, no. 4, pp. 76–82, 2018.

[17] Y. Cheng, Z. P. Song, X. X. Chang, and T. Wang, "Energy evolution principles of shock-wave in sandstone under unloading stress," *KSCE Journal of Civil Engineering*, vol. 24, no. 10, pp. 2912–2922, 2020.

[18] Y. Cheng, Z. P. Song, J. F. Jin, and W. Tong, "Waveform characterisation and energy dissipation of stress wave based on modified SHPB tests," *Geomechanics and engineering*, vol. 22, no. 2, pp. 187–196, 2020.

[19] Y. Cheng, Z. P. Song, W. X. Song, S. Wanxue, L. Shuguang, and Y. Tengtian, "Strain performance and fracture response characteristics of hard rock under cyclic loading," *Geomechanics and Engineering*, vol. 26, no. 6, pp. 551–563, 2021.

[20] J. Zhang, S. D. Lu, T. G. Feng, B. Yi, and J. Liu, "Research on reuse of silty fine sand in backfill grouting material and optimization of backfill grouting material proportions," *Tunnelling and Underground Space Technology*, vol. 130, Article ID 104751, 2022.

[21] S. H. Chen, H. X. Wei, and R. Q. Du, "Multi-resolution wavelet analysis of blasting vibration signals," *Rock and Soil Mechanics*, vol. 30, no. s1, pp. 135–139+143, 2009.

[22] M. S. Zhao, K. S. Liang, D. Y. Yu, Y. De-Yun, and R. Shao-Feng, "Effect of segments on time frequency characteristics of blasting vibration signals," *Journal of China Coal Society*, vol. 37, no. 1, pp. 55–61, 2012.

[23] A. M. Ekanem, J. Wei, X. Y. Li, M. Chapman, and I. Main, "P-wave attenuation anisotropy in fractured media: a seismic physical modelling study," *Geophysical Prospecting*, vol. 61, no. s1, pp. 420–433, 2013.

[24] L. F. Triviño, B. Mohanty, and B. Milkereit, "Seismic waveforms from explosive sources located in boreholes and initiated in different directions," *Journal of Applied Geophysics*, vol. 87, pp. 81–93, 2012.

[25] B. Song and Y. Cao, "Stability criterion of surrounding rock in roadway under blasting vibration load based on wavelet energy," *Rock and Soil Mechanics*, vol. 34, no. s1, pp. 234–240, 2013.

[26] X. N. Jia, Q. G. Jiang, M. C. He, F. Q. Ren, and S. Du, "Experimental research on acoustic emission spectral characteristics of granite strainbursts from Laizhou," *Chinese Journal of Underground Space and Engineering*, vol. 14, no. 1, pp. 51–57, 2018.

[27] E. D. H. Davies and S. C. Hunter, "The dynamic compression testing of solids by the method of the split Hopkinson pressure bar," *Journal of the Mechanics and Physics of Solids*, vol. 11, no. 3, pp. 155–179, 1963.

[28] X. B. Li, T. S. Lok, and J. Zhao, "Dynamic characteristics of granite subjected to intermediate loading rate," *Rock Mechanics and Rock Engineering*, vol. 38, no. 1, pp. 21–39, 2005.

[29] Y. Cheng, Z. P. Song, J. F. Jin, J. B. Wang, and T. T. Yang, "An experimental study on stress wave propagation and attenuation of sandstone during stress unloading process," *Journal of Vibration and Shock*, vol. 39, no. 8, pp. 151–158, 2020.

[30] C. P. Lu, L. M. Dou, N. Zhang et al., "Microseismic frequency-spectrum evolutionary rule of rock burst triggered by roof fall," *International Journal of Rock Mechanics and Mining Sciences*, vol. 64, pp. 6–16, 2013.

[31] J. M. Lifshitz and H. Leber, "Data processing in the split Hopkinson pressure bar tests," *International Journal of Impact Engineering*, vol. 15, no. 6, pp. 723–733, 1994.

[32] S. Yoshida, S. Furuya, and M. Nishida, "High speed impact test on rock specimens with a compressive stress pulse," *Engineering Fracture Mechanics*, vol. 210, no. s1, pp. 132–146, 2019.

[33] Y. Rao, Y. Y. Xia, and Y. G. Hu, "Influence of pre-splitting crack on spectrum distribution characteristics of blasting vibration," *Journal of Sound and Vibration*, vol. 36, no. 7, pp. 191–198, 2017.